Anharmonic RRKM Calculation for the Dissociation of $(H_2O)_2H^+$ and Its Deuterated Species $(D_2O)_2D^+$

Di Song,*,†,‡ Hongmei Su,*,† Fan-ao Kong,† and Sheng-Hsien Lin‡,§

Beijing National Laboratory for Molecular Sciences (BNLMS), Institute of Chemistry, Chinese Academy of Sciences, Beijing 100190, People's Republic of China, Institute of Applied Chemistry, Institute of Molecular Science, Chiao-Tung University, Hsin-Chu, Taiwan, Republic of China, and Institute of Atomic and Molecular Science, Academia Sinica, P.O. Box 23-166, Taipei, Taiwan, Republic of China,

Received: April 27, 2010; Revised Manuscript Received: August 2, 2010

Investigations on the dissociation kinetics of hydrated protonium ions, $(H_2O)_2H^+$ and their deuterated species $(D_2O)_2D^+$, are reported based on the harmonic and anharmonic oscillator model using the transition state theory and *ab initio* calculations. We find that the dissociation of $(H_2O)_2H^+$ and $(D_2O)_2D^+$ exhibits a distinct threshold behavior due to the existence of activation energies. Moreover, the deviation between the harmonic and anharmonic dissociation rate constants becomes larger in the high energy or temperature range, with the rate constants becoming unreasonably large under the harmonic oscillator model. The isotope effect is found to become more distinct but only in the case of the anharmonic oscillator model. These results show that the anharmonic Rice−Ramsperger−Kassel−Marcus (RRKM) theory can provide a reasonably good description for the dissociation of $(H_2O)_2H^+$ and $(D_2O)_2D^+$. Furthermore, a theoretical model to demonstrate the principle of vibrational predissociation spectroscopy (VPS) is established from the viewpoint of RRKM theory and applied in determining the experimental conditions and understanding the role of the dissociation rate constant $k(E)$ played in the VPS experiment, using $(H_2O)_2H^+$ and $(D_2O)_2D^+$ as examples.

1. Introduction

Hydrated hydronium ions are of broad interest because they serve as prototypical systems for the study of proton transfer in aqueous solutions which plays important roles in many chemical and biological processes. The protonated water dimer, $(H_2O)_2H^+$, has thus been extensively explored both experimentally and theoretically.[1−17] In the early 1950s, Nakahara, Saito, and Kuroya first suggested its existence in crystals of organic acids.[1] The symmetric $H_2O\cdot H^+\cdot H_2O$ structure in crystals was first determined by X-ray diffraction experiments in 1968.[2] Further evidence was later found later in both liquid-phase and gas-phase spectral experiments. The continuous absorption spectra of $H_5O_2^+$ and $D_5O_2^+$ ions were extracted from IR spectra of solutions of acids, which also presented a direct proof for complexes of the type $(A\cdots H^+\cdots A)$ being the simplest stable proton ion solvated in solutions of acids.[3] In the gas phase, Yeh et al. observed two band origins for the symmetric and asymmetric O−H stretch modes at 3608.8 and 3684.4 cm^{-1} with the vibrational predissociation spectroscopy (VPS).[4] In the region of the shared proton stretch, Asmis et al. and Fridgen et al. revealed the three strong bands of $(H_2O)_2H^+$ and $(D_2O)_2D^+$ between 620 and 1900 cm^{-1} by infrared multiphoton photodissociation (IRMPD) spectroscopy, which is also a type of VPS experiment.[5,6] Diken et al. and Headrick et al. also observed two intense bands in the $(H_2O)_2H^+\cdot Ar$ spectrum of the same region.[7,8]

On the other hand, most of the high-level electronic structure calculations have also confirmed that $(H_2O)_2H^+$ has a minimum energy structure with C_2 symmetry, in which the proton is shared by the two water groups.[9−17] This symmetric geometry was also used to obtain the properties of $(H_2O)_2H^+$, such as the harmonic frequencies, potential energy surface, and dissociation energy.

For the important IRMPD spectroscopy experiments[5,6] in probing the shared proton region of the potential energy surface and revealing the corresponding IR bands of stretching and bending fundamentals of $(H_2O)_2H^+$ and $(D_2O)_2D^+$, the key experimental procedures involved in monitoring the intensity of H_3O^+ or D_3O^+ ions formed by dissociation of $(H_2O)_2H^+$ or $(D_2O)_2D^+$ subsequent to the absorption of multiple IR photons are as shown in eq 1:

$$(H_2O)_2H^+ \xrightarrow{h\nu} [(H_2O)_2H^+]^* \xrightarrow{k(E)} H_3O^+ + H_2O \quad (1a)$$

$$(D_2O)_2D^+ \xrightarrow{h\nu} [(D_2O)_2D^+]^* \xrightarrow{k(E)} D_3O^+ + D_2O \quad (1b)$$

However, little is known about the kinetics of the dissociation of these protonated water dimers, and most experimental and theoretical studies focused on the spectral properties. In 1989, Yeh et al. estimated that the Rice−Ramsperger−Kassel−Marcus (RRKM) lifetimes of $(H_2O)_2H^+$ excited 0.1 kcal/mol above the dissociation limit were shorter than 10^{-6} s.[4] Recently, in the studies of the reactions of $(H_2O)_nH^+ + D_2O$ and $(D_2O)_nD^+ + H_2O$ ($n = 1-4$), Honma et al. reported the ratio of the isomerization and dissociation rate constants but they did not determine the absolute value of the dissociation rate constants.[18]

To unravel the kinetics of the unimolecular reaction of $(H_2O)_2H^+$ and its deuterated analogue $(D_2O)_2D^+$, in the paper we use the transition state theory to compute their dissociation rate constants separately under the harmonic and anharmonic

* To whom correspondence should be addressed. E-mail: songdi@iccas.ac.cn (D.S.); hongmei@iccas.ac.cn (H.S.).
† Chinese Academy of Sciences.
‡ Chiao-Tung University.
§ Academia Sinica.

10.1021/jp103782r
Published on Web 08/19/2010

models. In the IRMPD experiments, Asmis et al. and Fridgen et al. found no satisfactory agreement between the experimental spectrum of $(H_2O)_2H^+$ and its calculated harmonic frequencies in the region between 600 and 1600 cm^{-1}.[5,6] They suggested the shared proton of $(H_2O)_2H^+$ vibrates in a rather flat potential and will undergo a large amplitude motion, which results in the deviation from the harmonic oscillator model.[5] The failure of the harmonic picture for $(H_2O)_2H^+$ indicates the importance of the anharmonic effect. This is the reason why we take the anharmonic effect into account in this paper.

To our knowledge, the anharmonic effect on the potential surface has two aspects: One involves the modification of vibrational energy levels (or frequencies) of vibrational modes. Recent studies related to this anharmonic effect have been conducted in the electronic absorption and emission spectra, photophysical processes, unimolecular dissociations of molecules and clusters, and vibrational dynamics of liquid water.[16,19−23] The other aspect is related to the mode−mode coupling which can induce vibrational relaxation and modify the IR spectra through the appearance of side bands and the broadening of band-widths.[24] The adiabatic approximation model has been proposed to treat this mode−mode coupling effect. In this paper, we mainly use the Morse oscillator to describe the anharmonic effect on the modification of the energy levels which is closely related to the calculation of dissociation rate constants. The Morse oscillator model has turned out to be an effective way of treating the anharmonic effect in previous studies.[19,20]

In the RRKM calculations, obtaining the number and density of states is the key step. For the harmonic oscillator model, we use the direct state counting approach of the Beyer−Swinehart (B−S) algorithm.[25] However, because of the use of the Morse oscillator, the vibrational energy level expression is nonlinear and unsuitable for the B−S algorithm. This work therefore develops a new algorithm for counting the number and density of states under anharmonic approximation. Unlike the B−S algorithm used in the harmonic model,[25] in which the quantum numbers are continuous positive integers, the new algorithm is expected to solve the problem caused by limited quantum numbers in the quadratic energy expression. The average computational time of the program is at the level of minutes, depending on the scale of the total energy, numbers of vibrational modes, and anharmonic constants. Although the computational efficiency is lower than that of the B−S algorithm and the saddle point method (Y−L method),[21] this new algorithm can successfully implement the exact state counting approach for the anharmonic model.

After computing the dissociation rate constants of the protonated water dimers, we also attempt to establish a theoretical model to determine the role played by the microcanonical dissociation rate constant in the principle of VPS from the viewpoint of RRKM theory. The relationships between the VPS and the two rate constants, the IR optical absorption rate constant w and the RRKM dissociation rate constant $k(E)$, will be given. We expect that this work will provide the theoretical support for determining the experimental condition and the selection of the cluster ions to acquire the IR spectra in the VPS experiment.

This paper is organized as follows. The computational methods including calculations of unimolecular dissociation rate constants and the quantum chemistry calculations are given in Section 2, which also presents the basic principle of the interplay between VPS and w and $k(E)$. In Section 3, $(H_2O)_2H^+$ and $(D_2O)_2D^+$ are chosen as the examples to discuss the anharmonic and isotope effects on microcanonical and canonical cases and the role played by anharmonic rate constants on the principle of VPS. Finally, brief conclusions are given in Section 4.

2. Computational Methods and Theoretical Model

2.1. Microcanonical and Canonical Rate Constants. For a unimolecular reaction in the case of A* → A# → P, the microcanonical rate constant $k(E)$ with an internal energy E is given by the RRKM theory (often called quasi equilibrium theory) as

$$k(E) = \frac{\sigma}{h}\frac{W^{\#}(E - E^{\#})}{\rho(E)} \tag{2}$$

where σ is the reaction path degeneracy, h is Planck's constant, $\rho(E)$ represents the density of states of the energized reactant molecule A*, and $W^{\#}(E - E^{\#})$ denotes the total number of states for the activated complex A#, whose activation energy is $E^{\#}$. Thus, in essence, the RRKM theory is a statistical theory, based on the assumption that the rate of intramolecular vibrational energy redistribution is so rapid that the dynamical details are unimportant, and thus all energetically accessible quantum states will be populated equally. If one knows the potential energy surfaces (PESs), the molecular properties of the reactant and TS required in eq 2 could be determined and the microcanonical rate constant could be obtained.

Conventionally, the vibrational energy of the molecule is calculated under the harmonic approximation. However, for the dissociation of neutral and clusters ions, the anharmonic effect is significant. One way to take the anharmonic effect into account is to use the Morse oscillator model. In this case, we have

$$E_{n_i} = \left(n_i + \frac{1}{2}\right)\hbar\omega_i - \chi_i\left(n_i + \frac{1}{2}\right)^2\hbar\omega_i \tag{3}$$

where χ_i is the anharmonic constant, ω_i is the frequency of the ith vibrational mode, and n_i is the vibration quantum number of the vibrational mode. Equation 3 accounts well for the anharmonicity of the real bond, since the Morse oscillator energy level spacing decreases as the energy approaches the dissociation energy and the maximum quantum number n_i(max) exists. All the vibrational modes are treated anharmonically using the Morse oscillator model including the reaction coordinate, the O−O bond stretch mode.

In the evaluation of $W^{\#}(E - E^{\#})$ and $\rho(E)$, we use the direct state counting approach developed by the B−S algorithm in the harmonic oscillator model. However, in the anharmonic oscillator model, the energy level equation of E_{n_i} is parabolic rather than linear as in n_i. In such a case, we develop a new algorithm for implementing direct state counting under the anharmonic model. First, from each parabolic equation of E_{n_i}, we select an energy value whose n_i is less than or equal to n_i(max), respectively. Second, if the sum of the above energy values is not larger than the internal energy E of the energized reactant, we record this combination. Finally, the numbers of all the combinations represent the total number of states $W(E)$, and then $\rho(E) = ((dW(E))/dE)$ are determined. Similar procedures are used in the case of TS, and the total number of states for the TS, $W^{\#}(E - E^{\#})$, is also determined.

According to the transition state theory, the rate constant for unimolecular reactions in a canonical system can be given by

$$k(T) = \frac{kT}{h}\frac{Q^{\#}(T)}{Q(T)}\,e^{-(E^{\#}/kT)} \tag{4}$$

where $Q(T)$ and $Q^{\#}(T)$ represent the partition function for the reactant and the activated complex, respectively. Similarly, we shall also calculate the canonical rate constant using the harmonic and anharmonic model in this work.

2.2. *Ab Initio* Calculations and Variational Transition State Theory. Counting the number and density of vibrational states requires knowing the molecular properties of the reactant and TS complex. We thus optimize geometries of $(H_2O)_2H^+$ and $(D_2O)_2D^+$ by using the MP2 (full) method with the 6-311++G(2d,2p) basis set. The vibrational frequencies and the anharmonic constants χ_i have been obtained at the same calculation level.

The dissociation of $(H_2O)_2H^+$ or $(D_2O)_2D^+$ is a simple bond cleavage process, and no distinct TS exists in the dissociation process. In such a case, we use the variational transition state (VTST) approach to obtain the variational TS in the reaction by considering different positions for the TS along the reaction path, calculating their corresponding rate constants, and finding the minimal value.[19,20,26] In the microcanonical VTST, the minimal microcanonical rate constant is obtained along the reaction path according to the following equation:

$$\frac{dk(E)}{dq^{\#}} = 0 \tag{5}$$

where $q^{\#}$ is the reaction coordinate. In other words, a minimum value of $k(E)$ is searched for in numerous calculations of rate constants. Each calculation requires the optimized structure, single-point energy, zero-point energy (ZPE), and vibrational frequencies as functions of the reaction coordinate. All the quantum chemical calculations are carried out using the Gaussian 03 program.[27]

2.3. Theoretical Model for Vibrational Predissociation Spectroscopy. The vibrational predissociation spectroscopy (VPS) is an effective experimental method to observe the structure and nature of the cluster and cluster ions. There are three common types of VPS. The first one is the "messenger" type,[7,8,28] which assumes that a messenger species binds weakly to the cluster, resulting in small perturbations to the vibrations of the cluster. The cluster/messenger complex excited by an infrared laser undergoes vibrational predissociation losing the messenger, owing to intramolecular vibrational relaxation. The second type employs two lasers: a tunable infrared laser and a CO_2 laser.[4] The first tunable infrared laser is used, for example, to excite the O−H stretch of the molecule, and the second CO_2 laser is used to excite and dissociate the cluster by multiphoton processes. The VPS is obtained by monitoring the fragment ion signal as a function of the tunable IR laser frequency. Obviously, it is also feasible to use a single tunable pulsed laser to both excite and dissociate the cluster ions only if the photon energies absorbed is larger than the dissociation limit, which is the third type and this type of VPS is also referred to as infrared multiphoton dissociation (IRMPD) spectroscopy.[5,6,29,30]

Although the cluster ions follow different paths to being energized in the above three types of experiments, a basic reaction equation of the cluster ions can be expressed as

$$A \xrightarrow{w} A^* \xrightarrow{k(E)} B + C \tag{6}$$

where w denotes the molecular optical absorption rate constant. We shall describe the basic principle of the interplay between VPS and the rate constants of w and $k(E)$. In this work we shall use the dissociation of $(H_2O)_2H^+$ or $(D_2O)_2D^+$ as an example. It should be noted that rate equations more complicated than eq 6 can be proposed for different types of VPS but will still obtain similar results.

In the laser pulse duration τ of the laser (i.e., $0 < t \leq \tau$), $(H_2O)_2H^+$ becomes activated by the optical absorption and it may also undergo dissociation. The differential rate equations can be expressed as

$$\frac{dA}{dt} = -wA \tag{7}$$

$$\frac{dA^*}{dt} = wA - k(E)A^* \tag{8}$$

$$\frac{dB}{dt} = k(E)A^* \tag{9}$$

Equations 7−9 can easily be solved, and we obtain the expression for the concentration of the fragment product B,

$$B(t) = \frac{A_0}{k(E) - w}[k(E)(1 - e^{-wt}) - w(1 - e^{-k(E)t})] \tag{10}$$

where A_0 represents the initial concentration of the reactant A. At the end of the laser pulse, i.e., $t = \tau$, we will obtain the concentration of the activated molecule $A^*(\tau)$ and the product $B(\tau)$, respectively. When the laser pulse ends, i.e., $t < \tau$, the activated molecules continue the dissociation. In this case, the reaction equation can be modified by setting $w = 0$. This implies wA in eq 8 will disappear, and we obtain the new expression for the concentration of the product B,

$$B(t) = B(\tau) + \frac{wA_0}{k(E) - w}(e^{-w\tau} - e^{-k(E)\tau})(1 - e^{-k(E)(t-\tau)}) \tag{11}$$

To determine the relation between VPS and the rate constants of w and $k(E)$, we take the experimental condition into account and simplify eq 11.

If $w\tau \ll 1$, $k(E)\tau \ll 1$, and $k(E)t \gg 1$, then

$$B(t) = \frac{1}{2}A_0k(E)w\tau^2 + w\tau A_0 \approx w\tau A_0 \tag{12}$$

For $k(E)\tau \ll 1$, eq 12 shows that the yield of product B is a linear function of the IR absorption rate constant$w$. Under this condition, one can determine the IR spectrum of the cluster ions in the VPS experiment by measuring the yield of product B at various tunable IR laser frequencies ω_{IR}. Also, it should be noted that the total internal energy of E in the VPS experiment should be kept in a range larger than the activation energy $E^{\#}$, otherwise

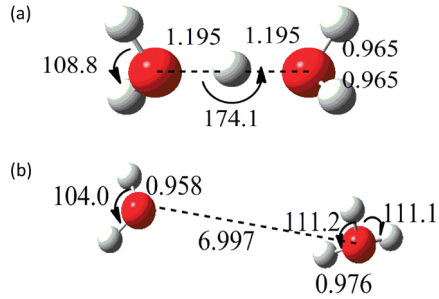

Figure 1. The optimized geometries of the stationary point (a) and transition state (b) for $(H_2O)_2H^+$ using MP2(full) 6-311++G(2d,2p) (bond lengths in angstroms and angles in degrees). The geometries of $(D_2O)_2D^+$ and the transition state are identical to those of $(H_2O)_2H^+$.

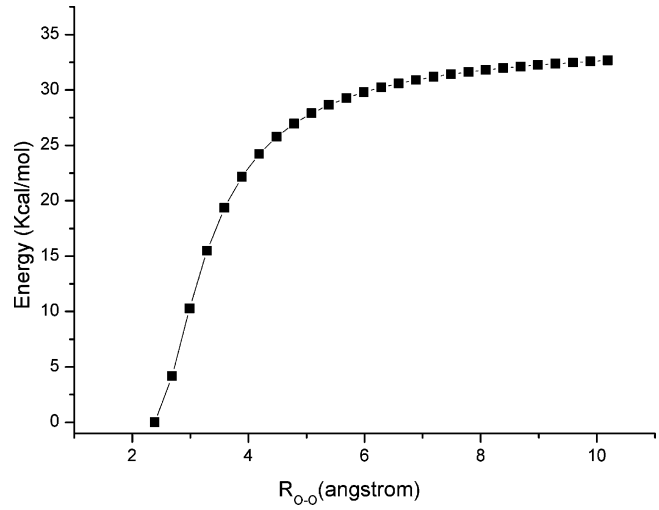

Figure 2. The potential energy curve of $(H_2O)_2H^+$ along the reaction coordinate.

$k(E)$ will be zero and the yield of product B will be zero with no signals detected.

3. Results and Discussion

3.1. Quantum Chemistry Calculation Results. Most previous theoretical studies have confirmed that the correct minimum of $(H_2O)_2H^+$ is of the C_2 symmetry, where the angle of $\angle OH^+O$ is not 180°, but the two bond distances of R_{H^+-O} are the same.[9−17] This means the structure of $(H_2O)_2H^+$ is like an equally shared proton "Zundel" complex which can form H_3O^+ fragments with both $O-H_2$ groups. Taking the previous theoretical studies into consideration, in this work we select the MP2 (full) method and 6-311++G(2d, 2p) basis set to optimize the geometry of $(H_2O)_2H^+$. In light of the Born−Oppenheimer (BO) approximation, the geometry of $(H_2O)_2H^+$ and $(D_2O)_2D^+$ is believed to be identical, which is shown in Figure 1. Table 1 lists the values of the electronic energy, the ZPE, O−O bond distance, the harmonic frequencies, and the anharmonic constants of $(H_2O)_2H^+$ and $(D_2O)_2D^+$. The geometry and harmonic frequencies of $(H_2O)_2H^+$ are in good agreement with the results of Frisch et al. and Honma et al.[9,18] and are only slightly different from the results obtained by Pudzianowski, Valeev et al., and Huang et al.[11,14,15] due to the different basis set or calculation method used. For the same reason, our harmonic frequencies of $(D_2O)_2D^+$ are also slightly different from those found by Kaledin et al.[12]

The properties of the activated complex are required in the calculation of the rate constant. However, no intrinsic TS exists for dissociation of $(H_2O)_2H^+$ and $(D_2O)_2D^+$ because the reverse process (i.e., the combination of hydronium ion and water) is barrierless. We use the microcanonical VTST to obtain the TS in the dissociation process. At first, the potential energy curve (PEC) was scanned by performing partial geometry optimization with fixed values of the reaction coordinate and all the other geometric parameters being optimized at the level of MP2(full)/6-311++G(2d,2p) (see Figure 2). The O−O bond lengths are the reaction coordinates for describing the dissociation process. Then, the vibrational frequencies and ZPEs of the optimized geometry calculated in each position of the PEC are employed to calculate the rate constant. Finally, the minimal $k(E)$ corresponding to the variational TS is determined to be located at a O−O bond distance of 6.977 Å. Thus, the activation energy of the variational TS is obtained to be 30.95 kcal/mol for the dissociation of $(H_2O)_2H^+$, which is consistent with the experimental values of 31.6 and 31.8 kcal/mol.[31,32] For the dissociation of $(D_2O)_2D^+$, the activation energy decreases slightly to 30.68 kcal/mol. All geometric and energetic parameters of the variational TS for $(H_2O)_2H^+$ and $(D_2O)_2D^+$ are collected in Table 1, and the geometry of the variational TS is given in Figure 1.

3.2. Anharmonic Effect and Isotope Effect. On the basis of the above *ab initio* calculation results, we calculate harmonic and anharmonic dissociation rate constants of $(H_2O)_2H^+$ and $(D_2O)_2D^+$ for the microcanonical and canonical cases, respectively. It is noted that the same TS in the PEC is used to perform the rate constant calculation in the microcanonical and canonical case, for the purpose of reducing the computational load. The results are listed in Tables 2 and 3 and illustrated in Figure 3,

TABLE 1: Properties of $(H_2O)_2H^+$ and $(D_2O)_2D^+$[a]

	$(H_2O)_2H^+$		$(D_2O)_2D^+$	
	minimum	transition state	minimum	transition state
harmonic frequencies	175, 298, 470, 545, 548, 621, 805, 1514, 1593, 1737, 1777, 3776, 3784, 3877, 3877	−24, 11, 41, 54, 157, 189, 925, 1672, 1715, 1717, 3611, 3713, 3721, 3863, 3977	126, 219, 341, 398, 415, 588, 594, 1104, 1164, 1270, 1305, 2727, 2737, 2855, 2855	−22, 8, 29, 38, 114, 142,700, 1223, 1245, 1246, 2570, 2728, 2734, 2785, 2914
anharmonic constants	0.0786, 0.0001, 0.0144, 0.0354, 0.0364, 0.0038, 0.0001, 0.0419, 0.0258, 0.0077, 0.0052, 0.0057, 0.0057, 0.0062, 0.0062	0.0002, 0.2085, 0.1672, 0.0051, 0.0001, 0.0894, 0.0112, 0.0076, 0.0077, 0.0079, 0.0119, 0.0130, 0.0112, 0.0121	0.0570, 0.0001, 0.0004, 0.0299, 0.0319, 0.0024, 0.0001, 0.0310, 0.0229, 0.0041, 0.0044, 0.0041, 0.0041, 0.0048, 0.0048	0.0001, 0.0551, 0.1204, 0.0115, 0.0001, 0.0673, 0.0083, 0.0061, 0.0062, 0.0055, 0.0097, 0.0100, 0.0080, 0.0093
electronic energy (Hartree)	−152.961 025	−152.911 631	−152.961 025	−152.911 631
zero-point energy (Hartree)	0.057 861	0.057 789	0.042 594	0.042 094
barrier[b] (kcal/mol))	32.66		32.66	
activation energy (kcal/mol)	30.95		30.68	

[a] The following values are calculated at the level of MP2 (full)/6-311++G (2d, 2p). Harmonic frequencies are in wavenumbers, and the bond distance is in angstroms. [b] Barrier (kcal/mol) is obtained without ZPE correction when the O−O bond distance R_{O-O} is 10.2 Å.

TABLE 2: Rate Constants of the Unimolecular Reaction: $(H_2O)_2H^+ \rightarrow H_3O^+ + H_2O$ for the Microcanonical and Canonical Cases

		microcanonical system		canonical system	
temperature (K)	corresponding energy (kcal/mol)	anharmonic rate constant (1/s)	harmonic rate constant (1/s)	anharmonic rate constant (1/s)	harmonic rate constant (1/s)
500	3.10			53.3	704.1
800	7.21			7.73×10^7	1.96×10^8
1200	14.16			4.55×10^9	2.03×10^{11}
1800	26.72			2.50×10^{11}	1.98×10^{13}
1985	30.95		5.92×10^6	3.76×10^{11}	4.62×10^{13}
1989	31.03	4.34×10^6	1.73×10^7	3.81×10^{11}	4.69×10^{13}
2000	31.29	1.27×10^8	1.85×10^8	5.36×10^{11}	4.91×10^{13}
2100	33.63	8.56×10^9	7.32×10^{10}	7.40×10^{11}	7.24×10^{13}
2200	36.00	3.58×10^{10}	6.67×10^{11}	9.88×10^{11}	1.03×10^{14}
2300	38.40	9.52×10^{10}	2.61×10^{12}	1.28×10^{12}	1.42×10^{14}
2400	40.82	1.95×10^{11}	6.98×10^{12}	1.63×10^{12}	1.90×10^{14}
2500	43.27	3.35×10^{11}	1.50×10^{13}	2.02×10^{12}	2.52×10^{14}
2600	45.27	5.27×10^{11}	2.80×10^{13}	2.47×10^{12}	3.20×10^{14}
2700	48.23	7.51×10^{11}	4.72×10^{13}	2.96×10^{12}	4.03×10^{14}
2800	50.73	9.97×10^{11}	7.35×10^{13}	3.49×10^{12}	4.99×10^{14}

TABLE 3: Rate Constants of the Unimolecular Reaction: $(D_2O)_2D^+ \rightarrow D_3O^+ + D_2O$ for the Microcanonical and Canonical Cases

		microcanonical system		canonical system	
temperature (K)	corresponding energy (kcal/mol)	anharmonic rate constant (1/s)	harmonic rate constant (1/s)	anharmonic rate constant (1/s)	harmonic rate constant (1/s)
500	4.38			298.6	1469.9
800	9.79			3.21×10^7	3.04×10^8
1200	18.60			1.58×10^{10}	2.62×10^{11}
1683	30.68	6.69×10^5	4.61×10^5	4.50×10^{11}	1.23×10^{13}
1700	31.11	8.88×10^7	5.92×10^7	4.88×10^{11}	1.35×10^{13}
1800	33.74	1.16×10^{10}	3.62×10^{10}	7.54×10^{11}	2.28×10^{13}
2000	39.09	1.86×10^{11}	1.57×10^{12}	1.56×10^{12}	5.54×10^{13}
2100	41.80	4.30×10^{11}	4.52×10^{12}	2.12×10^{12}	8.10×10^{13}
2200	44.53	8.26×10^{11}	1.03×10^{13}	2.79×10^{12}	1.14×10^{14}
2300	47.29	1.40×10^{12}	2.04×10^{13}	3.56×10^{12}	1.57×10^{14}
2400	50.05	2.16×10^{12}	3.63×10^{13}	4.45×10^{12}	2.09×10^{14}
2500	52.84	3.12×10^{12}	5.95×10^{13}	5.45×10^{12}	2.76×10^{14}
2600	55.63	4.26×10^{12}	9.18×10^{13}	6.55×10^{12}	3.48×10^{14}
2700	58.44	5.87×10^{12}	1.35×10^{14}	7.74×10^{12}	4.37×10^{14}
2800	61.26	7.43×10^{12}	1.89×10^{14}	9.02×10^{12}	5.39×10^{14}

respectively. The relationship between the total energy E of a microcanonical case and the temperature of a canonical case, which are listed in the first two columns of Tables 2 and 3, respectively, can be expressed as

$$E = -\left[\frac{\partial \ln Q(T)}{\partial \beta}\right] \tag{13}$$

where $\beta = 1/(kT)$. This means that the temperature range from 500 to 2800 K in the canonical case corresponds to the energy range from 3.10 to 50.73 kcal/mol for $(H_2O)_2H^+$ or from 4.38 to 61.26 kcal/mol for $(D_2O)_2D^+$ in the microcanonical case.

For $(H_2O)_2H^+$, as shown in Figure 3a, the dissociation occurs as the total energy reaches the activation energy, whether in the harmonic or anharmonic model. Furthermore, the harmonic and anharmonic rate constants sharply increase as the total energy becomes slightly higher than the activation energy. This indicates that, due to the activation energies in the dissociation of $(H_2O)_2H^+$, there exists a distinct threshold behavior in the plot of $k(E)$ as a function of E. The detailed data can be obtained from Table 2. At the activation energy of 30.95 kcal/mol, the harmonic dissociation rate constant of $(H_2O)_2H^+$ is 5.92×10^6 s^{-1}. When the anharmonic effect is considered, the activation energy increases to 31.03 kcal/mol, and the anharmonic rate constants at this energy is 4.34×10^6 s^{-1}. Whether the total energy is 30.95 or 31.03 kcal/mol, the time scales of the rate

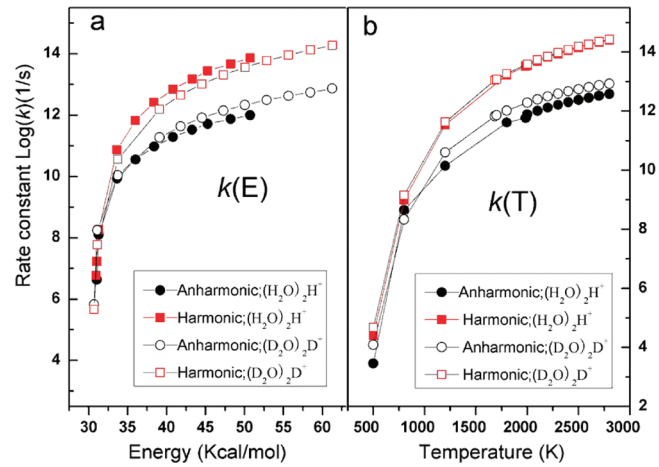

Figure 3. Dissociation rate constants of $(H_2O)_2H^+$ and $(D_2O)_2D^+$ in the (a) microcanonical case and (b) canonical case. The solid squares and circles represent harmonic and anharmonic rate constants for $(H_2O)_2H^+$, respectively. The hollow squares and circles shows the harmonic and anharmonic rate constants for the $(D_2O)_2D^+$, respectively.

constants are in agreement with the estimation of Yeh et al., who reported the RRKM lifetime of $(H_2O)_2H^+$ excited 0.1 kcal/mol above the dissociation limit was less than 1 μs.[4] However, it should be noted that the harmonic rate constant is nearly 4 times as large as the anharmonic rate constant at a total energy of 31.03 kcal/mol. Furthermore, Figure 3a gives us a distinct picture that the deviation between harmonic and anharmonic rate constants of $(H_2O)_2H^+$ becomes large when the total energy increases. Such a big difference is caused by the use of the different models, the harmonic and anharmonic potentials (the Morse potential), to describe the energy levels of vibrational bonds in the calculations. For instance, as shown in Figure 3a, the harmonic rate constants of $(H_2O)_2H^+$ always go up with the increasing total energy, because the harmonic RRKM calculations overestimate the number of states by using the linear quantum harmonic vibration equation. On the contrary, the anharmonic RRKM calculations of $(H_2O)_2H^+$ take into account the effect of the anharmonic Morse potential on the bond breaking whose rate constants tend to reach a plateau when the total energy increases beyond a certain limit. Similar results can be found in the canonical case as shown in Figure 3b.

The calculation results show that the anharmonic effect is very significant for the dissociation of $(H_2O)_2H^+$, which is consistent with a feature of $(H_2O)_2H^+$ in that the shared proton vibrates in a rather flat potential and undergoes large amplitude motion. From Table 2, we can also see that when the anharmonic rate constants of $(H_2O)_2H^+$ approach the limit of 10^{12} s^{-1}, its harmonic rate constants already reach 10^{13} s^{-1} and even 10^{14} s^{-1} with the increasing total energy or the temperature. According to the transition state theory, the RRKM lifetimes should be longer than the time scale of intramolecular vibrational relaxation ($10^{-13}-10^{-12}$ s). Thus, the harmonic results are obviously unreasonable, and the anharmonic effect should be considered in the calculations, especially in the high energy or temperature range.

The important anharmonic effect on the dissociation rate constant calculations is also manifested by the deuterated analogue $(D_2O)_2D^+$, according to Table 3 and Figure 3. The threshold behavior also exists for the dissociation of $(D_2O)_2D^+$. Furthermore, in the high total energy or temperature range, it can be seen from Figure 3 that, for both the microcanonical and canonical cases, the deviation between the harmonic model and the anharmonic model for $(H_2O)_2H^+$ is always larger than that for $(D_2O)_2D^+$, indicating that the anharmonic effect is more pronounced for $(H_2O)_2H^+$ than for $(D_2O)_2D^+$. This might be caused by the fact that the mass of the D atom is heavier than that of the H atom and thus the shared deuterium in $(D_2O)_2D^+$ is subject to a comparatively smaller amplitude of motion in the flat potential.

Moreover, as shown in Figure 3, the rate constants of $(D_2O)_2D^+$ calculated under the anharmonic model are always larger than those of the $(H_2O)_2H^+$ species at the same energy or temperature above the dissociation threshold, indicating the isotope effect on $(H_2O)_2H^+$ and $(D_2O)_2D^+$. However, for the harmonic model, the isotope effect nearly disappears, with the rate constants of $(D_2O)_2D^+$ being very close to those of $(H_2O)_2H^+$ in the canonical case or slightly smaller than those of $(H_2O)_2H^+$ in the microcanonical case. In other words, the isotope effect can only be observed when the anharmonic model is applied in the calculation. We speculate that the isotope effect might be weakened by overestimating the number of states in the harmonic rate constant calculations.

Overall, the above results imply that the anharmonic effect plays an important role in the dissociation of both $(H_2O)_2H^+$ and $(D_2O)_2D^+$. Moreover, the anharmonic effect on the dissociation of $(H_2O)_2H^+$ is more pronounced than that of $(D_2O)_2D^+$ owing to the larger anharmonic constants of $(H_2O)_2H^+$ than those of $(D_2O)_2D^+$. For the same reason, from the harmonic to the anharmonic model, the dissociation rate constants of $(H_2O)_2H^+$ drop down to a larger extent than those of $(D_2O)_2D^+$, resulting in a reversed isotope effect for the anharmonic rate constants. This isotope effect is exhibited more distinctively in the anharmonic oscillator model, indicating that a close correlation exists between the anharmonic effect and the isotope effect on the dissociation of $(H_2O)_2H^+$ and $(D_2O)_2D^+$.

3.3. Application to Vibrational Predissociation Spectroscopy. In Section 2.3, we discussed the interplay between VPS and the rate constants of w and $k(E)$ and established a theoretical model accounting for the basic principles of VPS. The model (eq 12) predicts that the IR spectrum of the cluster ion can be determined by measuring the yield of product B at various tunable IR laser frequencies ω_{IR} under the condition of $k(E)\tau \ll 1$. Although $k(E)$ finally disappears in eq 12, it should be emphasized that if the total internal energy of E is not above the activation energy $E^{\#}$, $k(E)$ will be zero and the product B cannot be observed. Thus, the total internal energy of E in the VPS experiment should be maintained above the activation energy $E^{\#}$ while fulfilling $k(E)\tau \ll 1$. These are two important features derived from the theoretical model for determining the experimental condition to measure IR spectra of the cluster ion and understanding the role of the dissociation rate constant $k(E)$ played in the VPS experiment. To illustrate the application of the theoretical model in VPS experiments, the clusters of $(H_2O)_2H^+$ and $(D_2O)_2D^+$ are chosen as examples and discussed as follows.

The discussion in Section 3.2 illustrated the importance of the anharmonic effect in the dissociation process. Thus, all the rate constants $k(E)$ in this section are calculated by using the anharmonic oscillator model. In the VPS experiment, the total energy E consists of two parts. One is the energy to resonantly excite each vibrational mode, corresponding to the energy given by the tunable IR laser with frequency ω_{IR}. The other is the energy of the multiphoton IR absorption for exciting and dissociating the cluster ions which, for convenience, is represented as the temperature T. Thus, this section of thermal energy can be calculated through eq 13, and the total energy E can be well-defined at a specific IR frequency ω_{IR} and a given temperature T. Subsequently, a series of rate constants $k(E)$ are calculated as a function of the total energy E. The logarithms of $k(E)$ are then plotted as a function of the IR frequency ω_{IR} at several typical temperatures and displayed in Figure 4b−d for $(H_2O)_2H^+$. Similar results for $(D_2O)_2D^+$ are shown in Figure 4b′−d′. Here, we adopt the IR frequencies ω_{IR} obtained from *ab initio* calculations which can conveniently provide a broadband IR spectra (shown in Figure 4a,a′) from 4000 cm^{-1} down to less than 500 cm^{-1}.

It is noteworthy here that the calculated logarithms of $k(E)$ displayed in Figure 4 does not denote the actual IR absorption intensity because, according eq 12, the VPS signal intensity is not proportional to $k(E)$. Rather, the purpose of calculating $k(E)$ at a specific IR frequency ω_{IR} and a given temperature T is to predict conditions for a specific vibrational mode to be observed in the VPS experiment, based on the principle that $k(E)$ should be above the dissociation threshold for the fragment ions to be detected. Therefore, as an example, the results shown in Figure 4 b,b′ indicate that only the high-frequency mode, the O−H stretch mode (>3550 cm^{-1} for $(H_2O)_2H^+$ and >2600 cm^{-1} for $(D_2O)_2D^+$) can be observed in the VPS experiment at about

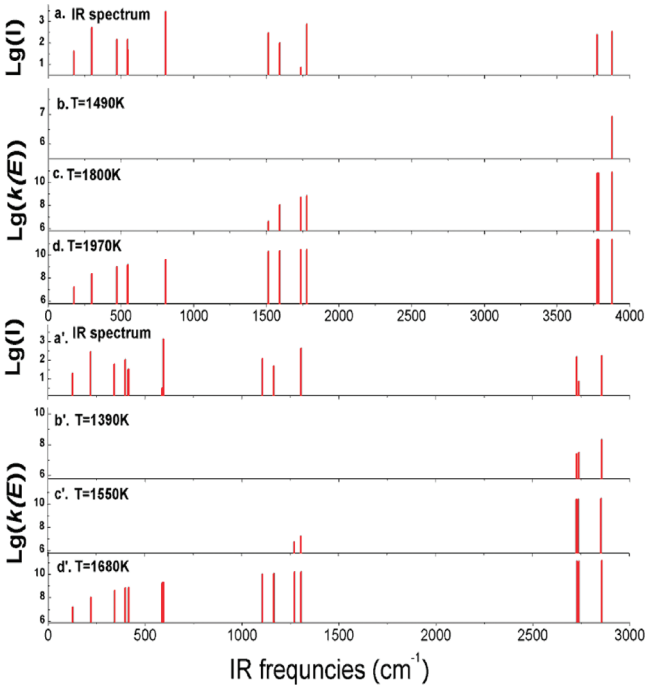

Figure 4. (a and a′) The logarithms of IR intensities as function of the frequencies for $(H_2O)_2H^+$ and $(D_2O)_2D^+$, respectively; ((b−d) and (b′−d′)) The logarithms of $k(E)$ as a function of IR laser frequencies for $(H_2O)_2H^+$ and $(D_2O)_2D^+$ at different temperatures, respectively.

1490 and 1390 K, respectively. It shows that the clusters, $(H_2O)_2H^+$ and $(D_2O)_2D^+$, need to be "heated" or absorb enough photon energy for dissociation and hence yield fragment ion signals in the VPS. Experimentally, Yeh et al.[4] observed the high frequency O−H stretch by using the second laser to "heat" the cluster ions.

Importantly, from Figure 4b−d, a general trend is revealed in that more vibrational modes can be observed in the spectrum as T increases. For example, at 1800 K, eight vibrational modes of $(H_2O)_2H^+$ between 1500 and 3900 cm^{-1} appear in Figure 4c. When T reaches 1970 K, all the vibrational frequencies for $(H_2O)_2H^+$ can be monitored (see Figure 4d). Similar results are also obtained in Figure 4b′−d′ for the case of $(D_2O)_2D^+$. Such a trend indicates that the cluster ions need to absorb enough IR photons to become "hotter" for observing the lower frequency vibrational modes. This conclusion agrees well with the actual VPS experiments performed by Asmis et al.[5] in which it was found that multiple IR photon absorption enabled the observation of the lower frequency modes between 620 and 1900 cm^{-1} and approximately 6−18 photons were absorbed for the cluster ions of $(H_2O)_2H^+$ to dissociate.

This theoretical approach can be applied to treat other cluster ions. As in the case of $(H_2O)_2H^+$ and $(D_2O)_2D^+$, this approach can be expected to provide the theoretical support to determine the experimental conditions for measuring the IR spectra of cluster ions in the VPS experiment.

4. Conclusions

We have investigated the dissociation kinetics of hydrated protonium ions, $(H_2O)_2H^+$ and their deuterated species $(D_2O)_2D^+$, based on the harmonic and anharmonic oscillator models using the transition state theory and *ab initio* calculations. In the RRKM calculations, the total number and density of states are evaluated through the direct state counting approach developed by the Beyer−Swinehart algorithm for the harmonic oscillator mode, and this work develops a new algorithm to implement the direct state counting approach for the anharmonic model. From the calculation results, we find that the dissociation of $(H_2O)_2H^+$ and $(D_2O)_2D^+$ exhibits a distinct threshold behavior due to the existence of activation energies. The anharmonic and harmonic dissociation rate constants are quite different when the total energy or temperature increases, and the rate constants even become unreasonably large when using the harmonic oscillator model for both clusters in the high energy or temperature range. These results imply that the anharmonic effect plays an important role in the dissociation of both $(H_2O)_2H^+$ and $(D_2O)_2D^+$. Moreover, because of the isotope effect, the anharmonic effect on the dissociation of $(H_2O)_2H^+$ is more pronounced than that of $(D_2O)_2D^+$. The isotope effect is exhibited more distinctly in the anharmonic oscillator model, indicating that the anharmonic effect and the isotope effect on the dissociation of $(H_2O)_2H^+$ and $(D_2O)_2D^+$ are closely correlated.

On the basis of the RRKM calculations, we have established a theoretical model to demonstrate the principle of vibrational predissociation spectroscopy and applied this model in determining the experimental conditions and in understanding the role that the dissociation rate constant $k(E)$ played in the VPS experiment, using $(H_2O)_2H^+$ and $(D_2O)_2D^+$ as examples. The results show that the clusters, $(H_2O)_2H^+$ and $(D_2O)_2D^+$, need to be "heated" or absorb enough photon energy to dissociate and hence yield fragment ion signals in the VPS experiment. Importantly, the model predicts that, for observing the lower-frequency vibrational modes, the cluster ions need to absorb more IR photons to become "hotter". These results are expected to provide theoretical support for the VPS experiment of other cluster ions as well.

Acknowledgment. This work was supported by the National Natural Science Foundation of China (Grant No. 20733005 and Grant No. 20973179), the National Basic Research Program of China, and the National Sciences Council of Taiwan.

References and Notes

(1) Nakahara, A.; Saito, Y.; Kuroya, H. *Bull. Chem. Soc. Jpn.* **1952**, *25*, 331.
(2) Olovsson, I. *J. Chem. Phys.* **1968**, *49*, 1063.
(3) Yukhnevich, G. V.; Tarakanova, E. G.; Mayorov, V. D.; Librovich, N. B.; Kurnakov, N. S. *J. Mol. Struct.* **1992**, *265*, 237.
(4) Yeh, L. I.; Okumura, M.; Myers, J. D.; Price, J. M.; Lee, Y. T. *J. Chem. Phys.* **1989**, *91*, 7319.
(5) Asmis, K. R.; Pivonka, N. L.; Santambrogio, G.; Brümmer, M.; Kaposta, C.; Neumark, D. M.; Wöste, L. *Science* **2003**, *299*, 1375.
(6) Fridgen, T. D.; McMahon, T. B.; MacAleese, L.; Lemaire, J.; Maitre, P. *J. Phys. Chem. A* **2004**, *108*, 9008.
(7) Diken, E. G.; Headrick, J. M.; Roscioli, J. R.; Bopp, J. C.; Johnson, M. A.; McCoy, A. B. *J. Phys. Chem. A* **2005**, *109*, 1487.
(8) Headrick, J. M.; Bopp, J. C.; Johnson, M. A. *J. Chem. Phys.* **2004**, *121*, 11523.
(9) Frisch, M. J.; Del Bene, J. E.; Binkley, J. S.; Schaefer, H. F. *J. Chem. Phys.* **1986**, *84*, 2279.
(10) Xie, Y. M.; Remington, R. B.; Schaefer, H. F. *J. Chem. Phys.* **1994**, *101*, 4878.
(11) Pudzianowski, A. T. *J. Chem. Phys.* **1995**, *102*, 8029.
(12) Kaledin, M.; Kaledin, A. L.; Bowman, J. M.; Ding, J.; Jordan, K. D. *J. Phys. Chem. A* **2009**, *113*, 7671.
(13) Kaledin, M.; Kaledin, A. L.; Bowman, J. M. *J. Phys. Chem. A* **2006**, *110*, 2933.
(14) Valeev, E. F.; Schaefer, H. F. *J. Chem. Phys.* **1998**, *108*, 7197.
(15) Huang, X. C.; Braams, B. J.; Bowman, J. M. *J. Chem. Phys.* **2005**, *122*, 044308.
(16) Vener, M. V.; Kühn, O.; Sauer, J. *J. Chem. Phys.* **2001**, *114*, 240.
(17) Vendrell, O.; Brill, M.; Gatti, F.; Lauvergnat, D.; Meyer, H. D. *J. Chem. Phys.* **2009**, *130*, 234305.
(18) Honma, K.; Armentrout, P. B. *J. Chem. Phys.* **2004**, *121*, 8307.
(19) Yao, L.; He, R. X.; Mebel, A. M.; Lin, S. H. *Chem. Phys. Lett.* **2009**, *470*, 210.

(20) Yao, L.; Mebel, A. M.; Lin, S. H. *J. Phys. Chem. A* **2009**, *113*, 14664.
(21) Yao, L.; Mebel, A. M.; Lu, H. F.; Neusser, H. J.; Lin, S. H. *J. Phys. Chem. A* **2007**, *111*, 6722.
(22) Shao, Y.; Yao, L.; Lin, S. H. *Chem. Phys. Lett.* **2009**, *478*, 277.
(23) Chaban, G. M.; Jung, J. O.; Gerber, R. B. *J. Phys. Chem.A* **2000**, *104*, 2772.
(24) (a) Lin, S. H. *J. Chem. Phys.* **1976**, *65*, 1053. (b) Hayashi, M.; Shiu, Y. J.; Liang, K. K.; Lin, S. H.; Shen, Y. R. *J. Phys. Chem. A* **2007**, *111*, 906225.
(25) Beyer, T.; Swinehart, D. F. *Commun. Assoc. Comput. Machin.* **1973**, *16*, 379.
(26) Kislova, V. V.; Nguyen, T. L.; Mebel, A. M.; Lin, S. H.; Smith, S. C. *J. Chem. Phys.* **2004**, *120*, 7008.
(27) Frisch, M. J.; Trucks, G. W.; Schlegel, H. B.; Scuseria, G. E.; Robb, M. A.; Cheeseman, J. R.; Montgomery, J. A., Jr.; Vreven, T.; Kudin, K. N.; Burant, J. C.; Millam, J. M.; Iyengar, S. S.; Tomasi, J.; Barone, V.; Mennucci, B.; Cossi, M.; Scalmani, G.; Rega, N.; Petersson, G. A.; Nakatsuji, H.; Hada, M.; Ehara, M.; Toyota, K.; Fukuda, R.; Hasegawa, J.; Ishida, M.; Nakajima, T.; Honda, Y.; Kitao, O.; Nakai, H.; Klene, M.; Li, X.; Knox, J. E.; Hratchian, H. P.; Cross, J. B.; Bakken, V.; Adamo, C.; Jaramillo, J.; Gomperts, R.; Stratmann, R. E.; Yazyev, O.; Austin, A. J.; Cammi, R.; Pomelli, C.; Ochterski, J. W.; Ayala, P. Y.; Morokuma, K.; Voth, G. A.; Salvador, P.; Dannenberg, J. J.; Zakrzewski, V. G.; Dapprich, S.; Daniels, A. D.; Strain, M. C.; Farkas, O.; Malick, D. K.; Rabuck, A. D.; Raghavachari, K.; Foresman, J. B.; Ortiz, J. V.; Cui, Q.; Baboul, A. G.; Clifford, S.; Cioslowski, J.; Stefanov, B. B.; Liu, G.; Liashenko, A.; Piskorz, P.; Komaromi, I.; Martin, R. L.; Fox, D. J.; Keith, T.; Al-Laham, M. A.; Peng, C. Y.; Nanayakkara, A.; Challacombe, M.; Gill, P. M. W.; Johnson, B.; Chen, W.; Wong, M. W.; Gonzalez, C.; Pople, J. A. *Gaussian 03*, revision B.01; Gaussian, Inc.: Wallingford, CT, 2003.
(28) Okumura, M.; Yeh, L. I.; Myers, J. D.; Lee, Y. T. *J. Phys. Chem.* **1990**, *94*, 3416.
(29) Lin, C. K.; Wu, C. C.; Wang, Y. S.; Lee, Y. T.; Chang, H. C.; Kuowb, J. L.; Klein, M. L. *Phys. Chem. Chem. Phys.* **2005**, *7*, 938.
(30) Chaudhuri, C.; Wang, Y. S.; Jiang, J. C.; Lee, Y. T.; Chang, H. C.; Niedner-Schatteburg, G. *Mol. Phys.* **2001**, *99*, 1161.
(31) Meot-Ner, M.; Speller, C. V. *J. Phys. Chem.* **1986**, *90*, 6616.
(32) Cunningham, A. J.; Payzant, J. D.; Kebarle, P. *J. Am. Chem. Soc.* **1972**, *94*, 7627.

JP103782R